Deciphering relationships between the Nicobar and Bengal Submarine Fans, Indian Ocean

Kevin T. Pickering [1], Andrew Carter [2], Sergio Andò [3], Eduardo Garzanti [4], Mara Limonta [4], Giovanni Vezzoli [4], Kitty L. Milliken [5]

[1] Earth Sciences, University College London (UCL), London WC1E 6BT, UK
kt.pickering@ucl.ac.uk

[2] Dept of Earth and Planetary Sciences, Birkbeck, University of London, Malet Street, Bloomsbury, London WC1E 7HX
a.carter@ucl.ac.uk

[3] Laboratory for Provenance Studies, Department of Earth and Environmental Sciences, University of Milano-Bicocca, 210126 Milano, Italy
sergio.ando@unimib.it
eduardo.garzanti@unimib.it
mara.limonta@unimib.it
giovanni.vezzoli@unimib.it

[4] Bureau of Economic Geology, Jackson School of Geosciences, The University of Texas at Austin, 2305 Speedway Stop C1160 Austin, TX 78712-1692, USA
kittym@utexas.edu

Keywords: Nicobar Fan, Bengal Fan, sediment provenance, IODP Expedition 362, Indian Ocean, Sunda Subduction Zone

Abstract

The Nicobar Fan and Bengal fans can be considered as the eastern and western parts, respectively, of the largest submarine-fan system in the world. This study presents the integrated results of petrographic and provenance studies from the Nicobar Fan, and evaluate these in the context of controls on sedimentation. Both fans were predominantly supplied by Himalaya-derived material. A lack of volcanic material in the Nicobar Fan rules out sources from the Sumatra magmatic arc. Overall, the petrographic data shows a progressive decrease in sedimentary detritus and corresponding increase of higher-grade metamorphic detritus up-section. Changes in sediment provenance and exhumation rates are seen to track changes in sediment mass accumulation rates (MARs). High sediment accumulation rates in the Bengal Fan occurred at ~14–13.5 Ma, with a switch to the Nicobar Fan at ~9.5 Ma. Distinct changes, common to both fans, occurred from 9.5–8.3 Ma (peak MARs) and 5.5–5.2 Ma (sharp drop in MARs). At ~5 Ma a drop in MARs observed in both fans coincided with a change in river drainage associated with the Brahmaputra diverting west of the uplifting Shillong Plateau. The Nicobar Fan at this time was supplied by an eastern drainage route that finally closed at ~2 Ma, when MARS in the Nicobar Fan significantly decreased. Sediment provenance record these changes in routing whereby Bengal Fan deposits include sources from the Namche Barwa syntaxis that are not present in the Nicobar Fan due to a more localised eastern drainage that included material from the Indo-Burma wedge. Prior to ~3 Ma source exhumation rates were rapid and constant and the short lag-time rules out significant intermediate storage and mixing. In terms of climate *versus* tectonic controls, tectonically driven changes in the river network have had most influence on fan sedimentation.

1. Introduction

The Bengal–Nicobar Fan, Indian Ocean (Fig. 1), has the greatest length and area of any submarine fan worldwide, and has been intensively studied to investigate the possible link between Himalayan tectonics and the Asian monsoon (Curray and Moore, 1971; France-Lanord *et al*., 2016). International Ocean Discovery Program (IODP) Expedition 362 sampled, for the first time, the full sedimentary succession of the Nicobar Fan west of North Sumatra (Fig. 1), and showed that starting at ~9.5 Ma, there was a dramatic and sustained rise in sediment accumulation rates (SARs) from 250–350 m/Myr until ~2 Ma that equalled or far exceeded those on the Bengal Fan at similar latitudes (McNeill *et al*., 2017a,b). This rise in SARs and a constant Himalayan-derived provenance indicates a major restructuring of the sediment routing in the Bengal–Nicobar submarine fan that was interpreted as coinciding with inversion of the Eastern Himalayan Shillong Plateau and encroachment of the west-propagating Indo–Burmese wedge, reducing continental accommodation space and increasing sediment supply directly to the Fan (*ibid*.). These results challenged the commonly held view that discrete tectonic or climatic events that impacted on the Himalayan–Tibetan Plateau caused the changes in sediment flux seen in the Bengal submarine fan.

A provenance contribution for the SGF sands from the only previously drilled fan deposits in the eastern Indian Ocean (DSDP Site 211), known as the "Investigator Fan", from the Sunda arc in the vicinity of the Andaman–Nicobar islands cannot be ruled out, but the indistinguishable nature of the sands from DSDP sites 211 and 218 (the latter being Bengal Fan deposits) suggests that they were derived from the same Himalayan source (Ingersoll and Suczek, 1979). Lithic populations of Bengal–Nicobar sands are dominated by metasedimentary rock types, with the abundant micas (predominantly muscovite and biotite), suggesting a provenance from uplifted crystalline basement terranes of granitic to granodioritic composition, as well as extensive low- to high-grade metasedimentary terranes (Ingersoll and Suczek, 1979). The Investigator Fan was likely a distal and, because of subduction-accretion processes, now an

isolated segment of the Nicobar Fan. The oldest recovered fan sediments are ~19 Ma mud-rich SGF deposits (Pickering *et al*., 2019).

Here, we present for the first time the integrated results of studies on sediments from the Nicobar Fan, and re-evaluate these in the context of both the Bengal and Nicobar fans, and in terms of previous studies of sediment provenance. Figure 2 shows the potential source areas for the sediments that are considered in this paper, and Figure 3 summarises the stratigraphic units defined from IODP Expedition 362. Whilst the Brahmaputra and Ganges rivers join on the delta plains of the Bengal Basin most sand in the Nicobar Fan is likely to be derived from the eastern Himalaya and the main Himalayan range as the Siang River before flowing as the Brahmaputra north of Shillong Plateau and turning south across the Bengal Basin.

In order to better understand sediment source and variations in sediment flux through time and build on the initial findings of the study by McNeill *et al*. (2017b) we conducted a more extensive analysis of IODP 362 samples from sites U1480 (Fig. 3) and U1481 that extend back to 15 Ma. In addition to detrital zircon U–Pb and heavy mineral and petrographic analyses we also applied detrital apatite fission track analysis to examine bedrock exhumation rates as this can help pinpoint sediment source areas. Detrital zircon U–Pb and apatite fission track (AFT) analyses were performed at the London Geochronology Centre at University College London, U.K. and heavy mineral and petrography data were analysed by the team at the laboratory for provenance studies, university of Milano–Bicocca, Italy. Full method details are provided in the supplementary sections.

3. RESULTS AND INTERPRETATION

In this section we highlight the main trends observed in the datasets. More complete descriptions of the data are provided in the supplementary section.

3.1. Petrography

Provenance interpretation based on composition alone is made difficult by potential influences of grain size, hydraulic sorting and modification by diagenesis. These potential influences are considered in relation to compositional trends. The succession in the Nicobar Fan can be subdivided in four petrofacies intervals (Fig. 4 and supplementary data), from top to bottom: Petrofacies A (age < 2.39 Ma) consists of upper fine-grained feldspatho-quartzose sand richest in plagioclase and heavy minerals; Petrofacies B (age between 8.2–2.39 Ma) consists of fine-grained feldspatho-quartzose to quartz-rich feldspatho- quartzose sand; Petrofacies C (age 8.2 Ma) consists of fine-grained litho-feldspatho-quartzose to quartz-rich feldspatho-quartzose sand with more sedimentary and low-rank metasedimentary lithic grains; Petrofacies D (age > 8.2 Ma) consists of lower fine-grained mainly feldspatho-litho-quartzose sand richest sedimentary and low-rank metasedimentary rock fragments.

Analysed samples are all fine-grained sands showing a coarsening-upward trend. Sand composition ranges from feldspatho-litho-quartzose to quartz-rich feldspatho-quartzose (Fig. 4). Metamorphics include quartz-mica, slate, quartz-sericite, phyllite, schist, and rare garnet-bearing or sillimanite-bearing schist and gneiss. Subordinate fragments include granitoids and sedimentary rocks (shale, sparite, dolomite, siltstone, chert, micrite). Volcanic, metavolcanic, metabasite, and ultramafic lithics are recorded only occasionally. Among accessory grains, biotite and subordinate muscovite are invariably common, representing together 11±5 % of total framework grains. Heavy-mineral concentration estimated by point-counting ranges from 0.6–4%.

Average compositions are not significantly different throughout the sampled cores but there are some noteworthy differences. Moderately rich amphibole-epidote-garnet assemblages are present in the upper part of the IODP Site 1480 core (< 8.2 Ma), with the highest relative abundance (Amp 59–65% tHMC) seen in samples 80F9 and 80F52 (3.8–1.98 Ma). By contrast, epidote-amphibole-garnet assemblages are poor in the lower part of IODP sites 1480 and 1481 (10–8.2 Ma). Both cores record minor levels of apatite, tourmaline, sillimanite, clinopyroxene,

zircon, titanite, staurolite, kyanite, rutile and rare chloritoid apart from the lower part of IODP sites 1480 and 1481where tourmaline and apatite are common. Average indices for IODP samples < 8.2 Ma (site 1480) and 1481) are; tHMC 4.0±1.4, ZTR 6±3, HCI index 5±2, and MMI 63±16. Broadly similar average values were measured in the older samples (10–8.2 Ma) from sites 1480 and 1481; tHMC, 1.9±0.9, the ZTR 11±5, the HCI 8±3, and the MMI index 37±19. Within samples the down-section decrease in MMI index and increase in the ZTR index (r =0.74 and 0.66) is a typical mineralogical feature of Himalayan-derived foreland-basin sediments (e.g., Szulc *et al*., 2006; Najman *et al*., 2012).

Both hydraulic-sorting processes and diagenesis may alter provenance signals. IODP Leg 362 core depths reached ~1,350 mbsf sufficient to observe diagenetic alteration and certain features are consistent with this including a progressive decrease in tHMC index with burial depth, from 4 to 1. Amphibole decreases from ~50% tHM to ~15%, while epidote increases from ≤ 20 to 48% tHM. Sillimanite becomes rare to absent at greater burial depths. Conversely, zircon, tourmaline, apatite, and chloritoid increase. However, not all minerals show the expected trends associated with diagenesis. Garnet, kyanite, staurolite, titanite, and rutile do not show significant changes with burial depth. If diagenetic alteration were important garnet concentrations would be expected to increase. A grain-size increase is observed throughout the section and a good positive correlation is observed between grain size and heavy-mineral concentration (r = 0.79, significance level 0.1%). Garnet correlates positively with grain size both in the upper part of IODP Site 1480 core (r = 0.72, significance level. 5%) and in the lower part of both IODP sites 1480 and 1481 (r= 0.81, significance level. 2%). Conversely, epidote reaches a maximum in the finest-grained sample 81A22 (10–8.5 Ma,), which is the one with lowest heavy-mineral concentration. The epidote/garnet ratio was controlled by grain size and hydraulic-sorting processes rather than diagensis.

Whilst the epidote/garnet ratio has been considered as a useful parameter to distinguish between Ganges and Brahmaputra river sediments (Heroy *et al*., 2003; Garzanti *et al*., 2010) it is

not possible to definitely identify changes in contributions from either the Ganges or Brahmaputra because of these grain-size effects. After integrating petrographic and heavy-mineral evidence, the most reasonable conclusion is that vertical compositional trends show the effect of both provenance change and diagenetic bias, and that an upward increase in higher-grade metamorphic detritus from the Himalaya took place in the last 5.5 Ma. The Sumatra magmatic arc is an unplausible candidate, because volcanic detritus remains very minor even in Petrofacies D. To gain more insight into sand provenance we examined detrital zircon U-Pb and detrital apatite fission track signatures. The combination of geochronology and thermochronology should help pinpoint source areas and constrain sediment routing history.

3.2. Detrital zircon U–Pb analysis

In total 32 samples were analyzed covering the time interval between 15.4–0.21 Ma. Most samples contained sufficient zircon to measure > 100 grain ages, sufficient to detect the main detrital age components (Table S1). Figures 5 and 6 presents the data in the form of KDE plots and multidimensional scaling maps (Vermeesch, 2013) based on calculated K–S distances between U–Pb age spectra, comparing Nicobar Fan sand samples from this study with possible source areas compiled from the literature (Campbell *et al*., 2005; Allen *et al*., 2008; Bracciali *et al*., 2016 and references therein; Gehrels *et al*., 2011; Limonta *et al*., 2017). Although potential source areas span the drainage network of the Ganges and Brahmaputra rivers, the latter is considered more important as the upper Yarlung-Brahmaputra River extends into the Lhasa terrane on the Tibetan Plateau formed from Cambrian-age granites, and Paleozoic and Mesozoic clastics intruded by Jurassic through Paleogene granitoids of the pre-collision Gangdese arc. Southwards are the four main tectonostratigraphic sequences of Himalayan rocks represented by (from north to south) Paleozoic and Mesozoic sedimentary rocks of the Tethyan Himalaya Sequence (THS), Late Neoproterozoic to Ordovician high-grade metamorphic and plutonic rocks of the Greater Himalaya Sequence (GHS) and Paleoproterozoic and older metasedimentary and

igneous rocks of the Lesser Himalaya Sequence (LHS). Neogene leucogranites span both the THS and GHS. The southernmost unit comprises Neogene foreland-basin sediments.

McNeill *et al*. (2017b) proposed that the Nicobar Fan results show a provenance from Brahmaputra River sands mixed with reworked Himalaya material originally deposited in the remnant ocean and Surma basins (Fig. 2). A detrital zircon U–Pb study of Bengal Fan sands from IODP 354 by Blum *et al*. (2018) found Himalayan sources including the eastern syntaxis but few samples represented a Ganges or Brahmaputra provenance end-member, and most samples could be explained by mixing between the two systems. Figure 5 compares KDE plots of detrital zircon U–Pb data from the Bengal Fan (Blum *et al*., 2018) and Nicobar Fan (this study). The two datasets share Himalayan sources and visually the age distributions appear similar but a more robust way to compare the age distributions are multidimensional scaling maps (Vermeesch, 2013) based on calculated K–S distances between U–Pb age spectra. If the Nicobar Fan sediments were simply the result of switching and mixing of the two river feeder systems the MDS map would not show any major differences between Nicobar and Bengal Fan samples.

The MDS map in Figure 6A compares both fan datasets along with modern sands from the Ganges and Brahmaputra rivers. The first observation to note is that the two fans plot separately with little overlap. Nicobar Fan samples show greater spread in the Y-axis compared to the Bengal Fan suggesting input from additional sources to those of the Bengal Fan. Blum *et al*. (2018) suggested that the Plio–Pleistocene Ganges and Brahmaputra delivered sand to IODP 354 sites independently but were later mixed, by delta-plain avulsions on the shelf, longshore drift or submarine gravity flows. The Bengal Fan data plot support mixing although most samples show a closer affinity to the Brahamputra River especially samples ≤ 3.2 Ma. Overall differences between the two fans are small. The KDE plots show fans share the same range of Himalayan source ages (Fig. 2) differing mainly in the proportions of source ages (mainly GHS, THS, LHS). A few of the youngest Bengal Fan sediments contain ages < 10 Ma diagnostic of the syntaxis region (Najman *et al*., 2019) that are missing from Nicobar Fan samples. Proterozoic aged

zircons are common in Miocene Bengal Fan samples and fit with a more constant contribution (albeit low) from LHS/Ganges sources compared to the Nicobar Fan.

To further explore differences between the Bengal and Nicobar Fan zircon data Figure 6B shows an MDS map that includes zircons from Oligocene–Pleistocene samples of the Surma Basin (peripheral Indo–Burma wedge). The Surma Basin tectono-stratigraphic units (from old to young; Barail, Bhuban, Bokabil, Tipam and Dupi Tila) share a Himalayan provenance dominated by GHS and Transhimalayan arc detritus with minor contributions from the LHS (especially in the Dupi Tila), ophiolite and possibly the eastern Himalayan or Lohit–Dianxi (Burma) batholiths (Najman *et al*., 2012; Bracciali *et al*., 2016). Also included are combined samples from the Himalayan foreland basin section at Dungsam Chu, eastern Bhutan considered to represent paleoBrahmaputra deposited after the rise of the Shillong Plateau that caused the river to re-route to the north and west (Govin *et al*. 2018). MDS map (Fig. 6A) shows that samples from both fans plot in common space until a branch of young Bengal Fan samples (< 3.2 Ma) plot lower down on the Y-axis along with the modern Brahmaputra. The MDS map in (Fig. 6C) show the same trend. Surma Basin units plot within both fans. To understand the nature of differences on the MDS plot figure (Fig. 6D) compares normalized percent contributions of the same age groups used by Blum *et al.* (2018) permitting direct comparison with Bengal Fan samples. The percentages are remarkably similar given the data were produced using different experimental procedures but there are some subtle differences that help explain the MDS plots. For example Nicobar Fan samples show a consistently higher proportion of ages between 400–600 Ma, typical of the GHS and graph (Fig. 6B) shows Bengal Fan samples < 4 Ma contain a significantly higher percentage of young grain ages (up to 13% compared to < 3 % in the Nicobar Fan), which explains the trend of young (< 3.2 Ma) Bengal Fan samples.

3.3 Detrital apatite fission track data

233 Apatite fission track data can help to discern source areas as AFT exhumation ages are
234 known to vary across the Himalayan arc (Thiede and Ehlers, 2013). Table 1 summarises the
235 detrital fission apatite fission track results and the raw data and analytical details are provided in
236 the supplementary section. Sample burial depths (max. 1,350 mbsf) and downhole temperatures
237 rule out post-depositional resetting confirmed by ages older or contemporaneous with deposition
238 age, hence the data reflect provenance. Numbers of measured grain ages varied due to
239 abundances of suitable apatite but in most cases were sufficient to define the principal age
240 component quantified using the minimum age model based on a four-parameter probability
241 distribution (Galbraith, 2005) implemented in DensityPlotter (Vermeesch, 2012). The minimum
242 age is a more robust indicator of youngest age components where single grain spontaneous tracks
243 have zero or low track counts. Samples with the same or similar deposition ages were combined.
244 Figure 7 is a plot of lag-time between sample depositional age and AFT age components each
245 diagnostic of the time taken for exhumation, routing and deposition within the Nicobar Fan. The
246 main population of apatites in all samples show a younging trend with a near to constant lag time
247 of 1–2 Myr that records rapid exhumation in the apatite source areas. This pattern rules out
248 significant intermediate storage prior to deposition within the Nicobar Fan. The second most
249 abundant population of Miocene age also shows a constant younging trend. Together these data
250 show that there was very little mixing going on within the submarine fan. If this were the case the
251 age components of older samples would also be present in younger sands and there would not be
252 any systematic trend.
253 Older grains with ages between 35±10 and 337±65 Ma were also present in some samples
254 mostly represented by single grains. Also shown in the table are the main populations of apatites
255 found in unreset Plio–Pleistocene foreland basins that characterize bedrock exhumation (mainly
256 GHS as apatite is uncommon in LHS rocks) at the time they were deposited (Chirouze *et al*.,
257 2013; Coutand *et al*., 2016). In all cases these data are closely similar to the dominant minimum
258 age population seen in fan samples of equivalent deposition age.

4. Discussion

Compositional data confirm that the Nicobar Fan was a major sink for Himalaya-derived material since the Miocene. Vertical compositional trends show the effect of both provenance change and diagenetic bias due to dissolution of less durable detrital minerals as well as grain size and hydraulic-sorting processes. As a consequence more durable heavy minerals, including zircon, tourmaline, apatite, garnet and epidote tend to be relatively enriched with increasing age and burial depth. Epidote tends to increase in finer-grained samples and where heavy-mineral concentration is lower, and likewise garnet increases in coarser-grained samples and where heavy-mineral concentration is higher. Despite such influences there is a clear upward increase in higher-grade metamorphic detritus from circa 5.5 Ma (mainly hornblende, epidote, garnet, apatite, clinopyroxene, tourmaline, sillimanite, kyanite, zircon, titanite, and rare staurolite and rutile) consistent with Himalayan sources. The origin of sedimentary to low-grade metasedimentary detritus, the importance of which decreases progressively upwards, has yet to be ascertained, and the rare volcanic detritus rules out the Sumatra magmatic arc as a major contributor. Petrographic data suggests that sandy sediments reaching the Bengal shelf, and the Bengal and Nicobar fans, most closely match in composition those of the Brahmaputra sediments (Thompson, 1974; Ingersoll and Suczek, 1979; Yokohama *et al*., 1990; Garzanti, 2019).

Comparison of Bengal and Nicobar Fan detrital zircon datasets showed they share the same range of Himalayan source ages (Fig. 2) but there are also differences. Some Bengal Fan samples included ages < 10 Ma diagnostic of the syntaxis region (Najman *et al*., 2019) that are missing from the Nicobar Fan. Proterozoic aged zircons are more common in Bengal Fan samples and fit with a more constant contribution from LHS/Ganges sources. Combined U–Pb and thermochronometry work on the Bengal Fan samples (Najman *et al*., 2019) also found a significant component of grains derived from the TransHimalaya, supplied by drainages associated with the upper reaches of the Yarlung–Brahmaputra River plus subordinate

contributions from erosion of the Indo–Burma ranges. Whilst this background signal appeared constant throughout the drilled section of the Bengal Fan notable differences in proportions of zircon ages were considered to reflect differences in the loci of sediment production possibly driven by climate change. Could the same be argued for the Nicobar Fan?

Both the Bengal and Nicobar Fans show significant temporal changes in sediment accumulation rates but the changes are not always synchronous as seen in figure 8 that compares sediment mass accumulation rates (MAR) for the two systems (after Pickering *et al*., 2019). Significant accumulation occurred earlier in the Bengal Fan (from ~13 Ma) but peak MARs were reached in both fans over the same time interval from ~9.5–8.3 Ma. Similarly both fans show a marked fall in MARs at ~5.5–5.2 Ma. After this sedimentation in the Bengal Fan remained low but in the Nicobar Fan it increased again from ~3.8 Ma and peaked between ~2.4–1.7 Ma, after which accumulation dramatically dropped to low rates until a small rise in the Late Pleistocene, also seen in the Bengal Fan. The two major changes seen in both Fans thus took place at 9.5–8.3 Ma and 5.5–5.2 Ma suggesting a common mechanism. Were such changes climate driven?

4.1 Influence of Climate

Following the end of the Middle Miocene climatic optimum (a period of relative warmth from 18–14 Ma), the deep-marine composite isotope compilation shows that the $\delta^{18}O$ record was characterised by a series of incremental steps at ~14.6, 13.9, 13.1, 10.6, 9.9, and 9.0 Ma, which have been attributed to progressive deep-water (high-latitude) cooling and/or glaciation episodes (Holbourn *et al*., 2013). The earlier part of this step-wise deterioration in global climate therefore includes the Nicobar Fan, with the so-called Late Miocene "*Carbonate Crash*" at ~11–9 Ma (Lyle *et al*., 2008). A high-resolution benthic isotope record in combination with paired mixed-layer isotope and Mg/Ca-derived temperature data, by Holbourn *et al*. (2018), show that a long-term cooling trend was synchronous with the intensification of the Asian winter monsoon and strengthening of the biological pump from ~7–5.5 Ma. The climate shift occurred at the end of a

311 decrease in global $\delta^{13}C$, suggesting that changes in the carbon cycle involving the terrestrial and
312 deep-ocean carbon reservoirs were likely instrumental in driving late Miocene climate cooling.
313 The start of cooler climate conditions culminated with ephemeral Northern Hemisphere
314 glaciations between 6.0–5.5 Ma (*ibid*.). From the above discussion, we conclude that although
315 there are significant changes in global climate that occurred during the accumulation of the
316 Nicobar Fan, none appear to uniquely bracket this time interval from ~9.5 Ma. This suggests
317 another more local primary causal process.

318 The South Asian (Indian) monsoon would have had most influence on fan sediment
319 source areas although the East Asian monsoon would have impacted on the easternmost region
320 including the syntaxis (Nanga Parbat). The relationship between annual rainfall and its temporal
321 distribution and erosion as a driver for increased sediment supply (Snyder *et al*., 2003) implies
322 that a stronger monsoon would generate increased physical erosion and fluvial transport and
323 therefore it would be expected to also increase accumulation rates in the submarine fans. At the
324 present-day the summer monsoon accounts for ~70% of annual rainfall in all catchments draining
325 into the Bay of Bengal but due to orographic forcing it focuses precipitation on the southern edge
326 of the Lesser and Greater Himalayan Sequences of the Himalaya. The high- elevation, high-
327 relief and usually dry areas are only affected by stronger monsoons and significant precipitation
328 only occurs in the syntaxial region during the winter season (Bookhagen and Burbank, 2010).

329 Whilst inception of the South Asian monsoon is associated with early growth of the
330 Himalaya, the most significant changes in monsoon intensity took place in the middle Miocene,
331 ~12.9 Ma, when the monsoon wind system began to develop a strength and intensity similar to
332 the present (Betzler *et al.,* 2016). Proxy data indicate that from 11 Ma the summer monsoon was
333 weak but had intensified across South and East Asia by 7 Ma (Wan *et al*., 2007; Gupta *et al*.,
334 2015). However, when the summer monsoon was weaker the winter monsoon would have been
335 stronger and Gupta *et al*. (2015) noted that higher sediment accumulation rates seen in the
336 Himalayan foreland (Siwaliks) from 11–7 Ma were probably linked to winter precipitation during

strong westerlies when summer monsoon winds were weaker. From ~7 Ma the long-term global cooling trend appears to have coincided with intensification of the Asian winter monsoon recorded by a long-term trend toward heavier benthic $\boldsymbol{\delta}^{18}$O maxima. The most intense maxima peaked between 5.8–5.5 Ma before reversing in the Pliocene (Holbourn *et al*. 2018).

Stronger winter monsoons in the Miocene means that erosion would tend to be more concentrated on the upper slopes and the eastern syntaxis region hence fan provenance should be biased towards these areas and that over time contributions from these sources should decrease as the summer monsoon strengthened. However, no obvious trend linked to monsoon changes is apparent within the two fan datasets. Bengal Fan thermochronological data (Najman *et al*., 2019) record constant lag-times between ~12–5 Ma associated with steady erosion of the GHS and syntaxial antiform plus a significant component of THS but there is also a constant and significant presence of LHS material. Proportions of GHS, THS and LHS do not change until after 4 Ma, post peak summer monsoon strength at ~5.5 Ma. After this time there is a significant increase in zircons with ages < 300 Ma and thermochronometry data record short lag-times (Blum *et al*., 2018; Najman *et al*., 2019) diagnostic of rapid exhumation of the eastern syntaxis (Najman *et al*., 2019). Whilst inception of rapid syntaxial exhumation is considered to have started between 7–5 Ma (Bracciali *et al*., 2016; Lang *et al*., 2016), extremely rapid exhumation rates have only been sustained in the Namche Barwa Syntaxis region since 5 Ma. At the present-day the syntaxis region is noteworthy as a major source of sediment entering the Brahmaputra River system. Sediment geochemistry, petrography, and thermochronology data from the Brahmaputra River and its tributaries suggest that 35–70% of the sediment flux of the Brahmaputra River were sourced in the Namche Barwa Syntaxis (Garzanti *et al*., 2004; Singh and France-Lanord, 2002; Stewart *et al*., 2008; Gemigani *et al*., 2018). By contrast Nicobar Fan samples record constant contributions from the GHS and THS but LHS material is not always present. Further, no evidence such as zircon ages < 10 Ma, was found to support significant input from the rapidly exhuming Namche Barwa massif of the eastern syntaxis.

Sediment accumulation in both fans reached their acme between ~9.5–8 Ma similar to major sedimentation in the Himalayan foreland that has been associated with a strong winter monsoon hence it may be that climate has influenced MARS in both fan systems. However, post 9 Ma MARS vary between the two fans and changes in sediment provenance do not show a close correspondence to the increase in monsoon intensity that took place between 11–5 Ma or, its subsequent weakening. This suggests differences in fan accumulation rates and provenance is due to other primary causal processes.

4.2 Tectonics

From the above discussion distinct changes in sediment accumulation, common to both fans, occurred between 9.5–8.3 Ma (peak MARs) and 5.5–5.2 Ma (sharp drop in MARs). Similarly both fans share a change in provenance between 5–3 Ma recorded by thermochronometry data that show a switch to rapid exhumation in the Bengal Fan and a significant slow down in the Nicobar Fan. This change coincided with low rates of accumulation in the Bengal Fan and a marked increase in the Nicobar Fan between 3.8–1.7 Ma. Are any of these changes linked to tectonics?

Perhaps the most important development was a change in the path of the palaeo-Brahmaputra River. Prior to ~5 Ma the palaeo-Brahmaputra River flowed directly south although from the late Miocene it would also have been pushed westwards by the expanding Indo–Burma wedge that also folded and exposed earlier sediments deposited in the foreland and remnant ocean basin including the Surma Basin. The Indo–Burma wedge is a thin-skinned fold-thrust belt formed by oblique convergence and accretion of sediments of the Ganges–Brahmaputra Delta (GBD) on the Indian plate with the Shan Plateau (Betka *et al*., 2018). The frontal fold-belt (Chittagong Hill Tracts) records ongoing deformation of Paleogene – present Himalayan sourced fluvial-deltaic sedimentary rocks of the GBD (Najman *et al*., 2012). These include the late Eocene to early Miocene Barail Formation and in the outermost belt Miocene shallow marine

deposits of the Surma Group, overlain by Tipam Group Miocene–Pliocene fluvial deposits and Pliocene–Quaternary Dupi Tila Group fluvial and alluvial deposits. These have been folded into a series of fault-cored antiforms separated by wide low relief synclinal valleys and were sourced from the Himalaya with a minor arc-derived component from either the Trans-Himalaya, or recycled from the arc-derived Paleogene Indo–Burman Ranges (Allen *et al*., 2008; Najman *et al*., 2012). Most of the deformation of this outer belt took place between 8–2 Ma based on zircon thermochronometry which limits deformation to < 8 Ma (Betka *et al*., 2018) and onlaps across a latest Pliocene marker bed on a submarine anticline that dates deformation of the frontal part of the wedge to ~2 Ma (Maurin and Rangin, 2009).

The significance of timing of westward encroachment of the fold belt, which is also seen in seismic mapping across the Surma Basin (Najman *et al*., 2012), is that it combined with uplift of the Shillong Plateau at 5.2–4.9 Ma (Govin *et al*., 2018), to divert the paleo-Brahmaputra westwards around the Shillong Plateau producing an axial east to west route along strike of the mountain front before turning south. This development is constrained by fluvial deposits along the Dungsam Chu, foreland section of eastern Bhutan that show arrival of Transhimalayan (Cretaceous–Eocene zircon U–Pb ages) detritus from ~5 Ma onwards (Govin *et al*., 2018). Although Brahamputra material now routed west of the Shillong plateau, a southerly drainage also remained open to the east of the plateau until ~2 Ma when westward encroachment of the fold belt reached the margins of the Shillong Plateau. Evidence for this is supported by seismic data and provenance of the Tipam Formation that was later recycled into the Dupa Tila Group (Najman *et al*., 2012). Neogene deposits of the Surma Basin do not record evidence of the rise and erosion of the eastern syntaxis domal pop-up until the late Pliocene–Pleistocene (Bracciali *et al*., 2016) which is the time by which the southerly drainage east of the plateau had become closed. This explains why the Nicobar Fan samples do not contain zircon U–Pb ages diagnostic of the syntaxis region (ages <10 Ma), whereas the Bengal Fan samples does.

The onset of major river diversions at ~5 Ma coincided with a marked drop in MARS seen in both fans (Fig. 8). However by 4 Ma accumulation rates in the Nicobar Fan increased again until ~2 Ma when there was another marked drop in accumulation rates that remained low thereafter. By contrast Bengal Fan accumulation rates remained low from ~5–0.5 Ma after which there was a small increase. McNeill *et al*. (2017b) suggested the drop from ~2 Ma supported the hypothesis that impingement of the NinetyEast Ridge on the Sunda Trench diverted the primary flux west of the ridge along with a concomitant rise in mid–late Pleistocene accumulation rates on the Bengal Fan (e.g., France-Lanord *et al*., 2016) but as discussed above a westward re-routing of the Brahmaputra River may also have played a role leading up to final collision of the ridge with the subduction zone that blocked sediment supply from the north (Curray and Moore, 1974).

Whilst the MAR data and detrital zircon U–Pb data suggest changes related to re-organisation of river routing to the fans the detrital AFT show a constant behaviour in terms of apatite sources until 2 Ma after which the data suggest a modest slowdown. The main age trend seen in the lag-time plot of figure 7 reflect a constant supply from a source area undergoing steady erosion through time and the short lag-time rules out significant intermediate storage and mixing. The source of apatites is indicated by unreset Siwalik foreland sediments in the Arunachal Pradesh, eastern Bhutan and Nepal. Here, sands of comparable deposition ages to Nicobar Fan samples yielded identical AFT ages (Table 1) and lag times (Fig. 7). In the Arunachal Pradesh sands with depositional ages between 0–2 Ma the dominant population of AFT ages range from 2.9±0.8 Ma to 4.0±0.9 Ma with a secondary population between 7–15 Ma (Chirouze *et al*., 2013). Similar ages are seen to the west in the foreland of Eastern Bhutan. Here, most dominant populations of unreset apatites record AFT ages between from 3.6 ± 0.8 Ma (youngest) up to 6.9±1.2 Ma (8 Ma sample) and secondary populations from 15–10 Ma (Coutand *et al*., 2016). By contrast modern bedrock AFT ages from the Shillong Plateau are older, ranging

439 from 12.6–8.6 Ma and up to 101 Ma (Biswas, 2007) which rules out this block as a major
440 sediment source for Nicobar Fan apatites.
441
442 **4.3 Implications for sediment supply**
443 The Nicobar Fan and Bengal fans can be considered as the eastern and western parts,
444 respectively, of an integrated submarine-fan system. Their constituent sediments have the same
445 provenance, whether delivered by the eastern or western routes from the Brahmaputra River. At
446 ~2 Ma, the eastern drainage route to the Nicobar Fan became closed to recycled material, at
447 which time the MARS in Nicobar Fan significantly decreased.
448 The earliest onset of high MARs in the Bengal Fan occurred at ~14–13.5 Ma, with a
449 switch to the Nicobar Fan at ~9.5 Ma (Fig. 9). The earliest high MARs in the Bengal Fan are
450 broadly consistent with the observed rapid increase in seawater $^{187}Os/^{188}Os$ and decrease in
451 seawater $^{87}Sr/^{86}Sr$ in the mid to late Miocene at ~16–11 Ma and interpreted as reflecting rapid
452 thrust belt advance and exhumation of the outer Lesser Himalaya (Colleps *et al*., 2018), i.e., a
453 tectonic cause. The earliest high MARs in the Nicobar Fan do not demand a similar tectonic
454 explanation in the Himalaya and associated northern source areas for sediment supply via the
455 Ganges–Brahmaputra drainage basin. They most likely reflect an autocyclic shift from the
456 importance of sediment routing in submarine channel systems in the west of the NinetyEast
457 Ridge (Bengal Fan) to an eastern predominance (Nicobar Fan). However, an inspection of the
458 MARs for the both the Bengal and Nicobar fans shows that the high MARs in the Bengal Fan do
459 not show a substantial decrease until ~8.5–8 Ma, at least 1 Myr after the dramatic increase in the
460 Nicobar Fan (Fig. 9), suggesting that other contributary factors, probably tectonic, maintained the
461 overall high sediment flux. For example, a comprehensive magnetostratigraphic and
462 sedimentologic study by Zhang *et al*. (2019) suggests that the evolution of the basins in the
463 northern Himalaya Mountains has involved the late Cenozoic (~10–8 Ma), onset of the rift basins
464 and their expansion (~8–3 Ma) before shrinking and termination of the basins (~3–1.7 Ma). They

interpreted this as due to an accelerated tectonic uplift of the Himalaya at ~10 Ma, and two deformational events at ~3 Ma and at ~1.7 Ma.

At ~5 Ma, a drop in MARs is observed in both the Nicobar Fan and Bengal fans. Also, at ~5 Ma, there was a change in river drainage to west of uplifting Shillong Plateau, but as seen in the provenance and from the seismic (Tipam Formation; Shrivastava *et al*., 1974; Sahoo and Gogoi, 2009; Sarma and Chutia, 2013), drainage remained open to the east of the Shillong Plateau.

At ~4–3.5 Ma, an increase in MARs in recorded in the Nicobar Fan, but the Bengal Fan MARs remained low. These younger increased MARs might be related to accelerated erosion in the Namche Barwa syntaxis with hysteresis effects. The inception of rapid syntaxial exhumation started between 7–5 Ma (Bracciali *et al*., 2016; Lang *et al*., 2016) and extremely rapid exhumation rates have been sustained in the Namche Barwa region since ~5 Ma. The syntaxis region is noteworthy as a major source of sediment entering the Brahmaputra. Studies using sediment geochemistry, petrography, and thermochronology data from the Brahmaputra and its tributaries estimate that 35–70% of the sediment flux of the Brahmaputra was sourced Namche Barwa (Enkelmann *et al*., 2011; Garzanti *et al*., 2004; Gemigani *et al*., 2018; Singh and France-Lanord, 2002; Stewart *et al*., 2008). Note that the Neogene Surma Basin does not record evidence of the rise and erosion of the domal pop-up until latest Pliocene–Pleistocene time (Bracciali *et al*., 2016) and that Nicobar Fan samples do not contain zircon U–Pb ages diagnostic of this region (ages < 10 Ma), whereas Bengal Fan samples do.

Since ~10 Ma, global sea level has generally fallen (Miller *et al*., 2005), thereby decreasing accommodation on the shelf, and thus amplifying the processes driving sediment southward into the deep Indian Ocean. A fundamental question, however, is what caused the submarine routing system to favour the Nicobar Fan over the Bengal Fan since ~9.5–2 Ma?

5. Conclusions

U–Pb age spectra of detrital zircons, sand petrography and heavy-mineral analysis confirm that the Nicobar Fan was a major sink for Himalaya-derived material. Our data show the Nicobar Fan sands are similar but not identical to Bengal Fan sands. The Nicobar Fan sands lack young zircons from the eastern syntaxis. These are present in Bengal Fan sands deposited after < 3 Ma. This timing coincides with the group of Bengal Fan samples that show closest affinity to the Brahmaputra River and is also the time when the Brahamputra River re-routed to a modern configuration. The Nicobar Fan samples show AFT ages consistent with erosion of the frontal Himalaya and/or erosion of similar age foreland sediments.

The petrographic data suggests that supply from the metamorphic axial core of the Himalayan range has increased in the last 5.5 Ma The down-core decrease in heavy-mineral concentration and in the proportion of transparent heavy minerals relative to the heavy fraction also may be an effect of intrastratal solution, and even partly a grain-size effect. The coarsening-upward trend indicated by the studied samples would explain the upward decrease in the epidote/garnet ratio. Apatite fission track data shows that source area exhumation, routing and burial were extremely rapid from ~8–3 Ma. This broadly corresponds to a time of fan re-organisation. We interpret this latter signal as due to both rapid rapid exhumation in the source area and global cooling with lowered mean sea level. The more distant Investigator Fan and the thick accretionary prism of the Sunda subduction zone also include significant amounts of Himalaya-derived material delivered to the easternmost Indian Ocean (Oligocene–late Miocene).

We conclude that although there are significant changes in global climate that occurred during the accumulation of the Nicobar Fan, none appear to uniquely bracket the time interval from ~9.5 Ma when high and sustained MARs began. Similar arguments can be made for the Bengal Fan. Since ~5 Ma tectonically driven changes in the river network most influenced fan sedimentation and provenance and these changes can account for the main differences seen between the Bengal and Nicobar Fan, no doubt enhanced by the global deterioration in climate

516 and associated eustatic sea-level falls, to enhance the sediment flux to the Nicobar and Bengal
517 fans.
518
519 **References**
520
521 Allen, R., Najman, Y., Carter, A., Barfod, D., Bickle, M.J., Chapman, H.J., Garzanti, E., Vezzoli,
522 G., Andò, S. and Parrish, R. 2008. Provenance of the Tertiary sedimentary rocks of the Indo-
523 Burman Ranges, Burma (Myanmar): Burman arc or Himalayan-derived? *Journal of the*
524 *Geological Society London*, **165**, 1045–1057.
525
526 Betka, P.M., Seeber, L., Thomson, S.N., Steckler, M.S., Sincavage, R. and Zoramthara, C. 2018.
527 Slip-partitioning above a shallow, weak décollement beneath the Indo-Burman accretionary
528 prism. *Earth and Planetary Science Letters*, **503**, 17–28.
529
530 Betzler, C. *et al*. 2016. The abrupt onset of the modern South Asian Monsoon winds. *Science*
531 *Report*, **6**, 29838; doi: 10.1038/srep29838.
532
533 Biswas, S., Coutand, I., Grujic, D., Hager, C., Stockli, D. and Grasemann, B., 2007. Exhumation
534 and uplift of the Shillong plateau and its influence on the eastern Himalayas: new constraints
535 from apatite and zircon (U–Th–[Sm])/He and apatite fission track analyses. *Tectonics*, **26**,
536 TC6013.
537
538 Bracciali, L., Parrish, R.R., Najman, Y., Smye, A.J., Carter, A. and Wijbrans, J.R. 2016. Plio-
539 Pleistocene exhumation of the eastern Himalayan syntaxis and its domal 'pop-up'. *Earth Science*
540 *Reviews*, **160**, 350–385.
541

542 Blum, M., Kimberly Rogers, K., Gleason, J., Najman, Y., Cruz, J. and Fox, L. 2018. Allogenic
543 and autogenic signals in the stratigraphic record of the deep-sea Bengal Fan. *Nature Scientific*
544 *Reports*, **8**, 7973. doi:10.1038/s41598-018-25819-5.
545
546 Bookhagen, B. and Burbank, D.W. 2010. Toward a complete Himalayan hydrological budget:
547 Spatiotemporal distribution of snowmelt and rainfall and their impact on river discharge. *Journal*
548 *of Geophysical Research*, **115**, F03019, doi:10.1029/2009JF001426
549
550 Campbell, I.H., Reiners, P.W., Allen, C.M., Nicolescu, S. and Upadhyay, R. 2005. He–Pb double
551 dating of detrital zircons from the Ganges and Indus Rivers: Implication for quantifying sediment
552 recycling and provenance studies. *Earth and Planetary Science Letters*, **237**, 402–432.
553
554 Chirouze, F., Huyghe, P., van der Beek, P., Chauvel, C., Chakraborty, T., Dupont-Nivet, G. and
555 Bernet, M. 2013. Tectonics, exhumation, and drainage evolution of the eastern Himalaya since13
556 Ma from detrital geochemistry and thermochronology, Kameng River, Section, Arunachal
557 Pradesh. *Geological Society of America Bulletin*, **125**, 523–538.
558
559 Colleps, C.L., Ryan McKenzie, N., Stockli, D.F., Hughes, N.C., Singh, B.P., Webb, A.A.G.,
560 Myrow, P.M., Planavsky, N.J. and Horton, B.K. 2018. Zircon (U-Th)/He Thermochronometric
561 constraints on Himalayan thrust belt exhumation, bedrock weathering, and Cenozoic seawater
562 chemistry. *Geochemistry, Geophysics, Geosystems*, **19**, 257–271.
563
564 Coutand, I., Barrier, L., Govin, G., Grujic, D., Hoorn, C., Dupont-Nivet, G. and Najman, Y.
565 2016. Late Miocene-Pleistocene evolution of India-Eurasia convergence partitioning between the
566 Bhutan Himalaya and the Shillong Plateau: New evidences from foreland basin deposits along
567 the Dungsam Chu section, eastern Bhutan. *Tectonics*, **35**, 2963–2994.

Curray, J.R. 1991. Possible greenschist metamorphism at the base of a 22-km sedimentary section, Bay of Bengal. *Geology*, **19**, 1097–1100.

Curray, J.R. and Moore, D.G. 1971. Growth of the Bengal deep-sea fan and denudation in the Himalayas. *Geological Society American Bulletin*, **82**, 563–572.

France-Lanord, C., Spiess, V., Klaus, A. and the Expedition 354 Scientists 2016. *Neogene and late Paleogene record of Himalayan orogeny and climate: a transect across the Middle Bengal Fan. International Ocean Discovery Program Expedition*, **354,** Preliminary Report, Bengal Fan.

Galbraith, R.F. 2005. Statistics for Fission Track Analysis. Interdisciplinary Statistics Series, 224 pp. Chapman and Hall/CRC.

Garzanti, E. 2016. From static to dynamic provenance analysis - sedimentary petrology upgraded. *Sedimentary Geology*, **336**, 3–13.

Garzanti, E., Vezzoli, G., Andò, S., France-Lanord, C., Singh, S.K. and Foster, G. 2004. Sand petrology and focused erosion in collision orogens: the Brahmaputra case. *Earth and Planetary Science Letters*, **220**, 157–174.

Garzanti, E., Andó, S., France-Lanord, C., Vezzoli, G. and Najman, Y. 2010. Mineralogical and chemical variability of fluvial sediments. 1. Bedload sand (Ganga-Brahmaputra, Bangladesh). *Earth and Planetary Science Letters*, **299**, 368–381.

Garzanti, E. 2019. The Himalayan Foreland Basin from collision onset to the present: a sedimentary–petrology perspective. *In*: Treloar, P.J. and Searle, M.P. (eds), *Himalayan Tectonics: A Modern Synthesis*. Geological Society, London, Special Publications, **483**, 65–122.

Geersen, J., Bull, J.M., McNeill, L.C., Henstock, T.J., Gaedicke, C., Chamot-Rooke, N. and Delescluse, M. 2015. Pervasive deformation of an oceanic plate and relationship to large >MW8 intraplate earthquakes: The northern Wharton Basin, Indian Ocean. *Geology*, **43**, 359–362.

Gehrels, G., Kapp, P., DeCelles, P., Pullen, A., Blakey, R., Weislogel, A., Ding, L., Guynn, J., Martin, A., McQuarrie, N. and Yin, A. 2011. Detrital zircon geochronology of pre-Tertiary strata in the Tibetan-Himalayan orogen. *Tectonics*, **30**, 1944–1994.

Gemignani, L., van der Beek, P.A. Braun, J., Najman, Y., Bernet, M., Garzanti, E. and Wijbrans, J.R. 2018. Downstream evolution of the thermochronologic age signal in the Brahmaputra catchment (eastern Himalaya): Implications for the detrital record of erosion. *Earth and Planetary Science Letters*, **499**, 48–61.

Govin, G., Najman, Y., Dupont-Nivet, G., Millar, I., van der Beek, P., Huyghe, P., O'Sullivan, P., Mark, C. and Vögell, N. 2018. The tectonics and paleo-drainage of the easternmost Himalaya (Arunachal Pradesh, India) recorded in the Siwalik rocks of the foreland basin. *American Journal of Science*, **318**, 764–798.

Gupta, K., Yuvaraja, A., Prakasam, M., Clemens, S. C. and Velu, A. 2015. Evolution of the South Asian monsoon wind system since the late Middle Miocene. *Palaeogeography., Palaeoclimatology. Palaeoecology.* **438**, 160–167.

619 Heroy, D.C., Kuehl, S.A. and Goodbred, S.L. 2003. Mineralogy of the Ganges and Brahmaputra
620 Rivers: implications for river switching and Late Quaternary climate change. *Sedimentary*
621 *Geology*, **155**, 343–359.
622
623 Holbourn, A., Kuhnt, W., Clemens, S., Prell, W. and Andersen, N. 2013. Middle to late Miocene
624 stepwise climate cooling: evidence from a high-resolution deep water isotope curve spanning 8
625 million years. *Paleoceanography*, **28**, 688–699.
626
627 Holbourn, A.E., Kuhnt, W., Clemens, S.C., Kochmann, K.G.D., Jöhnck, J., Lubbers, J. and
628 Andersen, N. 2018. Late Miocene climate cooling and intensification of southeast Asian winter
629 monsoon. *Nature Communications*, doi: 10.1038/s41467-018-03950-1.
630
631 Ingersoll, R.V. and Suczek, C.A. 1979. Petrology and provenance of Neogene sand from Nicobar
632 and Bangal fans, Deep Sea Drilling Project Sites 211 and 218. *Journal of Sedimentary Petrology*,
633 **49**, 1217–1228.
634
635 Jena B., Kurian, P.J. and Avinash, K. 2016. Morphology of submarine channel-levee systems in
636 the eastern Bay of Bengal near Andaman region. *Journal of Coastal Conservation*, **20**, 211–220.
637
638 Lang, K.A., Huntington, K.W., Burmester, R. and Housen, B. 2016. Rapid exhumation of the
639 eastern Himalayan syntaxis since the late Miocene. *Geological Society of America Bulletin*, **128**,
640 1403–1422. Doi:10.1130/B31419
641
642 Limonta, M., Resentini, A., Carter, A., Bandopadhyay, P.C. and Garzanti, E. 2017. Provenance
643 of Oligocene Andaman sandstones (Andaman–Nicobar Islands): Ganga–Brahmaputra or
644 Irrawaddy derived? *In*: Bandopadhyay, P.C. and Carter, A. (eds), *The Andaman–Nicobar*

Accretionary Ridge: Geology, Tectonics and Hazards, 143–154. Geological Society London Memoir, **47**.

Lyle, M., Barron, J., Bralower, T.J., Huber, M., Lyle, A.O., Ravelo, A.C., Rea, D.K. and Wilson, P.A. 2008. Pacific Ocean and Cenozoic evolution of climate. *Reviews in Geophysics*, **46**, RG2002, doi:10.1029/2005RG000190.

Maurin, T. and Rangin, C. 2009. Structure and kinematics of the Indo-Burmese Wedge: Recent and fast growth of the outer wedge. *Tectonics*, **28**, TC2010, doi:10.1029/

McNeill, L.C., Dugan, B., Petronotis, K.E., Backman, J., Bourlange, S., Chemale, F., Chen, W., Colson, T.A., Frederik, M.C.G., Guèrin, G., Hamahashi, M., Henstock, T., House, B.M., Hüpers, A., Jeppson, T.N., Kachovich, S., Kenigsberg, A.R., Kuranaga, M., Kutterolf, S., Milliken, K.L., Mitchison, F.L., Mukoyoshi, H., Nair, N., Owari, S., Pickering, K.T., Pouderoux, H.F.A., Yehua, S., Song, I., Torres, M.E., Vannucchi, P., Vrolijk, P.J., Yang, T. and Zhao, X. 2017a. Expedition 362 methods. *In*: McNeill, L.C., Dugan, B., Petronotis, K.E., and the Expedition 362 Scientists, *Sumatra Subduction Zone. Proceedings of the International Ocean Discovery Program*, **362**, Sumatra Subduction Zone. College Station, TX (International Ocean Discovery Program). https://doi.org/10.14379/iodp.proc.362.102.2017

McNeill, L.C., Dugan, B., Backman, J., Pickering, K.T., Pouderoux, H.F.A., Henstock, T.J., Petronotis, K.E., Carter, A., Chemale, F. Jr., Milliken, K.L., Kutterolf1, S., Mukoyoshi1, H., Chen, W., Kachovich, S., Mitchison, F.L., Bourlange, S., Colson, T.A., Frederik, M.C.G., Gilles Guèrin, G., Hamahashi, M., House, B.M., Hüpers, A., Jeppson, T.N., Kenigsberg, A.R., Kuranaga, M., Nair, N., Owari, S., Shan, Y., Song, I., Torres, M.E., Paola Vannucchi, P., Vrolijk, P.J., Yang, T., Xixi Zhao, X. and Thomas, E. 2017b. Understanding Himalayan erosion and the

671 significance of the Nicobar Fan. *Earth and Planetary Science Letters,* **475**,134–142.
672 doi:10.1016/j.epsl.2017.07.019
673
674 Miller, K.G, Kominz, M.A., Browning, J.V., Wright, J.D., Mountain, G.S. and Katz, M.E. 2005.
675 The Phanerozoic record of global sea-level change. *Science*, **310**, 1293–1298.
676
677 Mitchell, A., Chung, S.L., Oo, T., Lin, T.H. and Hung, C.H. 2012. Zircon U–Pb ages in
678 Myanmar: Magmatic–metamorphic events and the closure of a neo–Tethys ocean. *Journal of*
679 *Asian Earth Sciences*, **56**, 1–23.
680
681 Najman, Y., Allen, R., Willett, E, Carter, A, Barford, D., Garzanti, E, Wijbrans, J., Bickle, M.,
682 Vezzoli, G., Ando, S., Oliver, G and Uddin, M.J. 2012, 'The record of Himalayan erosion
683 preserved in the sedimentary rocks of the Hatia Trough of the Bengal Basin and the Chittagong
684 Hill Tracts, Bangladesh'. *Basin Research*, **24**, 499– 519.
685
686 Najman, Y., Mark, C., Barfod, D.N., Carter, A., Parrish, R., Chew, D. and Gemignani, L. 2019.
687 Spatial and temporal trends in exhumation of the Eastern Himalaya and syntaxis as determined
688 from a multitechnique detrital thermochronological study of the Bengal Fan. *Geological Society*
689 *of America Bulletin*, **131**, 1607–1622.
690
691 Pickering, K.T., Pouderoux, H., McNeill, L.C., Backman, J., Chemale, F., Kutterolf, S., Milliken,
692 K.L., Mukoyoshi, H., Henstock, T.J., Dugan, B. and Stevens, D.E. 2019. Sedimentology,
693 stratigraphy and architecture of the Nicobar Fan (Bengal Depositional System), Indian Ocean:
694 Results from IODP Expedition 362. *Sedimentology*, in press.
695
696 Robinson, R.A.J., Brezina, C.A., Parrish, R.R., Horstwood, M.S.A., Oo, N.W., Bird, M.I.,

Thein, M., Walters, A.S., Oliver, G.J.H. and Zaw, K. 2014. Large rivers and Orogens: the evolution of the Yarlung Tsangpo–Irrawaddy system and the eastern Himalayan syntaxis. *Gondwana Research*, **26**, 112–121

Sahoo, M. and Gogoi, K.D. 2009. Depositional history, processes and mechanism of early Miocene sediments of Upper Assam Basin. *Journal of the Geological Society of India*, **73**, 575–585.

Sarma, J.N. and Chutia, A. 2013. Petrography of sub-surface Tipam Sandstone Formation of a part of Upper Assam Basin, India. *Global Research Analysis*, **2**, 112–113.

Shrivastava, P.K., Ganeshan, S. and Ray, D. 1974. Tipam Group in the Subsurface of Upper Assam Valley, South of Brahmaputra. *Journal of the Geological Society of India*, **15**, 165–181.

Singh, S.K., France-Lanord, C. 2002. Tracing the distribution of erosion in the Brahmaputra watershed from isotopic compositions of stream sediments. *Earth and Planetary Science Letters*, **202**, 645–662.

Snyder, N.P., Whipple, K.X., Tucker, G.E. and Merrits, D.J. 2003. Importance of a stochastic distribution of floods and erosion thresholds in the bedrock river incision problem, *Journal Geophysical Research*, **108**(B2), 2117, doi:10.1029/2001JB001655

Stewart, R.J., Hallet, B., Zeitler, P.K., Malloy, M.A., Allen, C.M. and Trippett, D. 2008. Brahmaputra sediment flux dominated by highly localized rapid erosion from the easternmost Himalaya. *Geology*, **36**, 711–739.

723 Thiede, R.C. and Ehlers, T.A. 2013. Large spatial and temporal variations in Himalayan
724 denudation. *Earth and Planetary Science Letters*, **371**, 278–293.
725
726 Thompson, R.W. 1974. Mineralogy of sands from the Bengal and Nicobar fans, sites 218 and
727 211, eastern Indian Ocean. *In*: von der Borch, C.C., Sclater, J.G. *et al*. (eds), Initial Reports of the
728 Deep Sea Drilling Project, **22**, 711–713. United States Government Printing Office, Washington,
729 DC.
730
731 Vermeesch, P. 2012. On the visualisation of detrital age distributions. *Chemical Geology*, **312-**
732 **313**, 190–194, doi: 10.1016/j.chemgeo.2012.04.021.
733
734 Vermeesch, P. 2013, Multi-sample comparison of detrital age distributions. *Chemical Geology*,
735 **341**, 140– 146.
736
737 Wan, S., Li, A., Clift, P.D. and Stuut, J-B.W. 2007. Development of the East Asian monsoon:
738 mineralogical and sedimentologic records in the northern South China Sea since 20 Ma.
739 *Palaeogeography, Palaeoclimatology, Palaeoecology*, **254**, 561–582.
740
741 Yokohama, K., Amano, K., Taira, A. and Saito, Y. 1990. Mineralogy of silts from the Bengal
742 Fan. *In*: Cochran, J.R., Stow, D.A.V. *et al*. (eds) Proceedings of the Ocean Drilling Program,
743 Scientific Results, **116**, 59–73. Ocean Drilling Program, College Station, Texas.
744
745 Zhang, W., Zhang, D., Fang, X., Zhang, T., Chen, C. and Yan, M. 2019. New paleomagnetic
746 constraints on rift basin evolution in the northern Himalaya mountains. *Gondwana Research*, **77**,
747 98–110.
748

List of figures

Figure 1. Regional map of the Bengal Depositional System composed of the Bengal Fan, The Nicobar Fan and the Investigator Fan. The map includes the deep-marine sedimentary system with fans separated by ridges, the Ganges–Brahmaputra River system, and relevant DSDP/ODP/IODP drill sites. No identifiable Bengal Fan sediments were found at DSDP Site 213, and DSDP Site 215 shows a hiatus from lower Eocene clay and nannofossil ooze to lower Miocene silty clay, that Curray (1991) interpreted as distal Bengal Fan sediments. DSDP Site 211 has a hiatus from non-fossiliferous clays overlying Maastrichtian to Pliocene strata, again probably distal fan sediments. The Investigator Fan, where Site 211 is located, is called after the Investigator Ridge. Channels recognised on the seafloor are reported after Curray and Moore (1971). Top right inset is a bathymetry map of the seafloor around IODP Expedition 362 sites (modified from Geersen *et al*., 2015); note the presence of well-identified channel heading south. The black box at ~10°N shows the study area of Jena *et al*. (2016) who proved the connection between channel E7 in the Bengal Fan and the Nicobar Channel.

Figure 2. Geology of potential source areas for the sediments in the Nicobar and Bengal submarine fans. Modified after Mitchell *et al*., 2012 and Robinson *et al*., 2014.

Figure 3. Schematic summary of lithostratigraphic units and subunits defined during IODP Expedition 362 in Holes U1480E–U1480G. Drilling in the nearby Hole U1481 recovered core from Units II and III. Sand-prone intervals were defined from a synthesis of sand-size fraction in recovered cores. Modified from McNeill *et al*. 2017a.

Figure 4. QFL diagram showing the progressive upward change of detrital modes, from feldspatho-litho-quartzose Petrofacies D (grey) and litho-feldspatho-quartzose Petrofacies C (yellow), to quart-rich feldspatho-quartzose Petrofacies B (orange), and eventually feldspatho-quartzose Petrofacies A (red). In Petrofacies D, the grey colour of the symbols becomes darker with depth; conversely, colours become brighter up-section in symbols of other petrofacies. Classification fields after Garzanti (2016).

775 **Figure 5**: Sample detrital zircon U–Pb age distributions plotted as adaptive kernel density
776 estimates (Vermeesch, 2013), comparing data from this study with Bengal Fan dataset of Blum *et*
777 *al*. (2018) and representative river sands from the Ganges and Brahmaputra rivers.
778 **Figure 6**. (**A**) Multidimensional scaling maps (MDS) comparing zircon U–Pb datasets for the
779 Nicobar and Bengal Fans, Ganges and Brahmaputra rivers (data from Blum *et al*., 2018). Pink
780 circles show BF, brown Nicobar Fan and blue river samples. Numbers refer to sample age (Ma).
781 Note the branch of Bengal Fan samples that most closely resemble the modern Brahmaputra are
782 all ≤ 3. 2 Ma. (**B**) This trend is caused by a higher percentage of grain ages < 50 Ma in the BF
783 samples. (**C**) MDS map comparing fan samples with stratigraphic units of the Surma Basin
784 (yellow) and Pliocene Himalayan foreland sediments (green) from the Dungsam Chu section
785 eastern Bhutan (Govin *et al*., 2018). (**D**) Compares the percentage contributions using the age
786 groups of Blum *et al.* (2018).
787 **Figure 7**. Graph showing lag-time relationships between sample depositional age and youngest
788 population of apatite fission track ages for samples from the Nicobar Fan and unreset Siwalik
789 foreland sediments.
790 **Figure 8**. Mass accumulation rates (MARs) calculated by Pickering *et al*. (2019).
791 **Figure 9**. Links between submarine-fan MARS and palaeogeographic and drainage changes
792 since the late Miocene. Fan reconstructions after McNeill *et al*. (2017) and upper three maps
793 show major river drainage changes adapted from Govin *et al*. (2018), Najman *et al*. (2012).
794 Arrows link palaeogeographic maps with relevant parts of the MAR graph for both the Nicobar
795 and Bengal fans.
796
797 **List of tables**
798 **Table 1:** Summary of AFT results. Samples of similar deposition age shown in italics were
799 combined for age component modelling. Included for comparison are the main provenance ages

800 of unreset Siwalik foreland sediments of comparable deposition age (Chirouz *et al.,* 2013;

801 Coutand *et al*., 2016). Errors on ages are 1sigma.

Figure 1

Click here to download Figure: Fig1_Pickering_et_al 2019.pdf

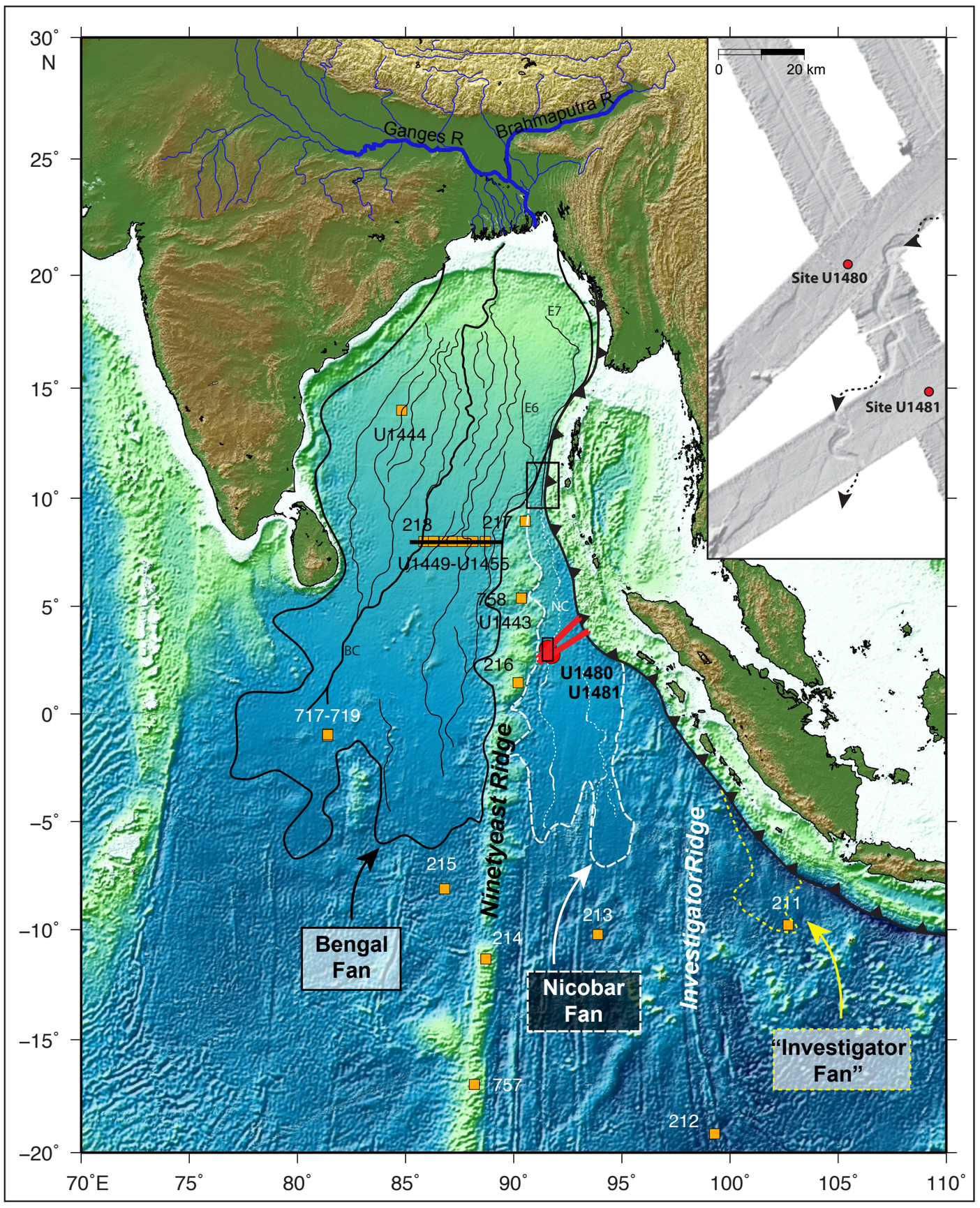

Figure 2

Click here to download Figure: Fig2_Pickering et al.pdf

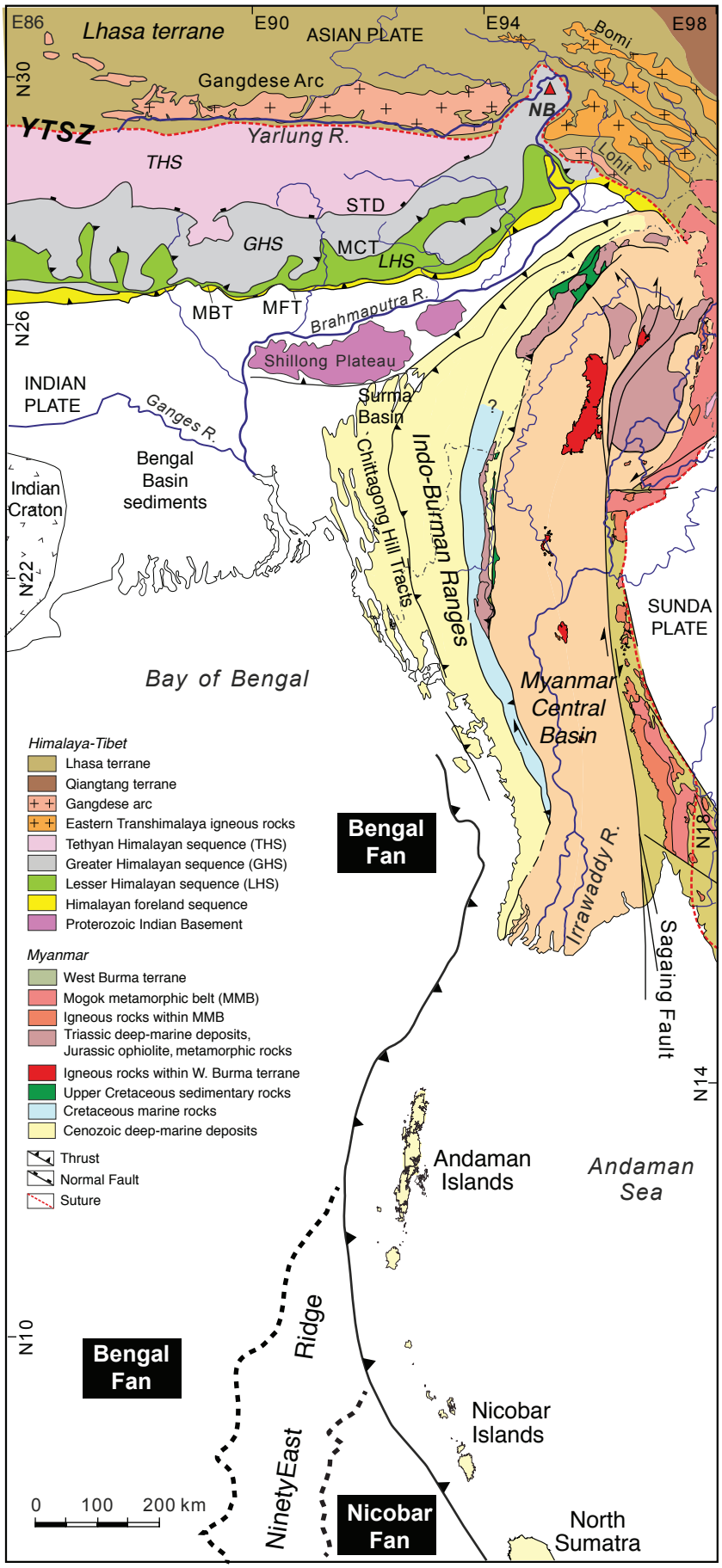

Figure 3

Click here to download Figure: Fig3_Pickering et al.pdf

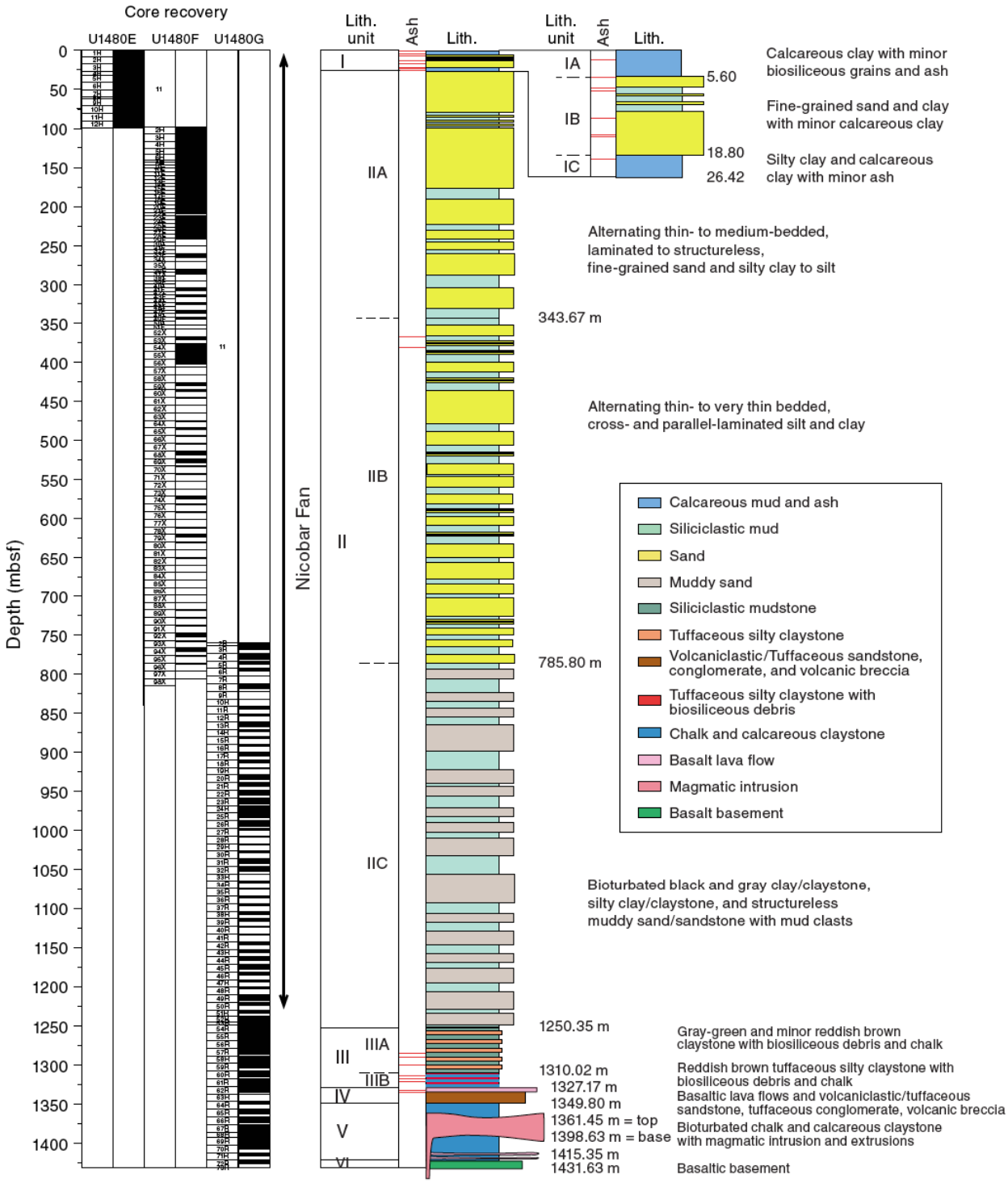

Figure 4

Click here to download Figure: Fig4_Pickering et al.pdf

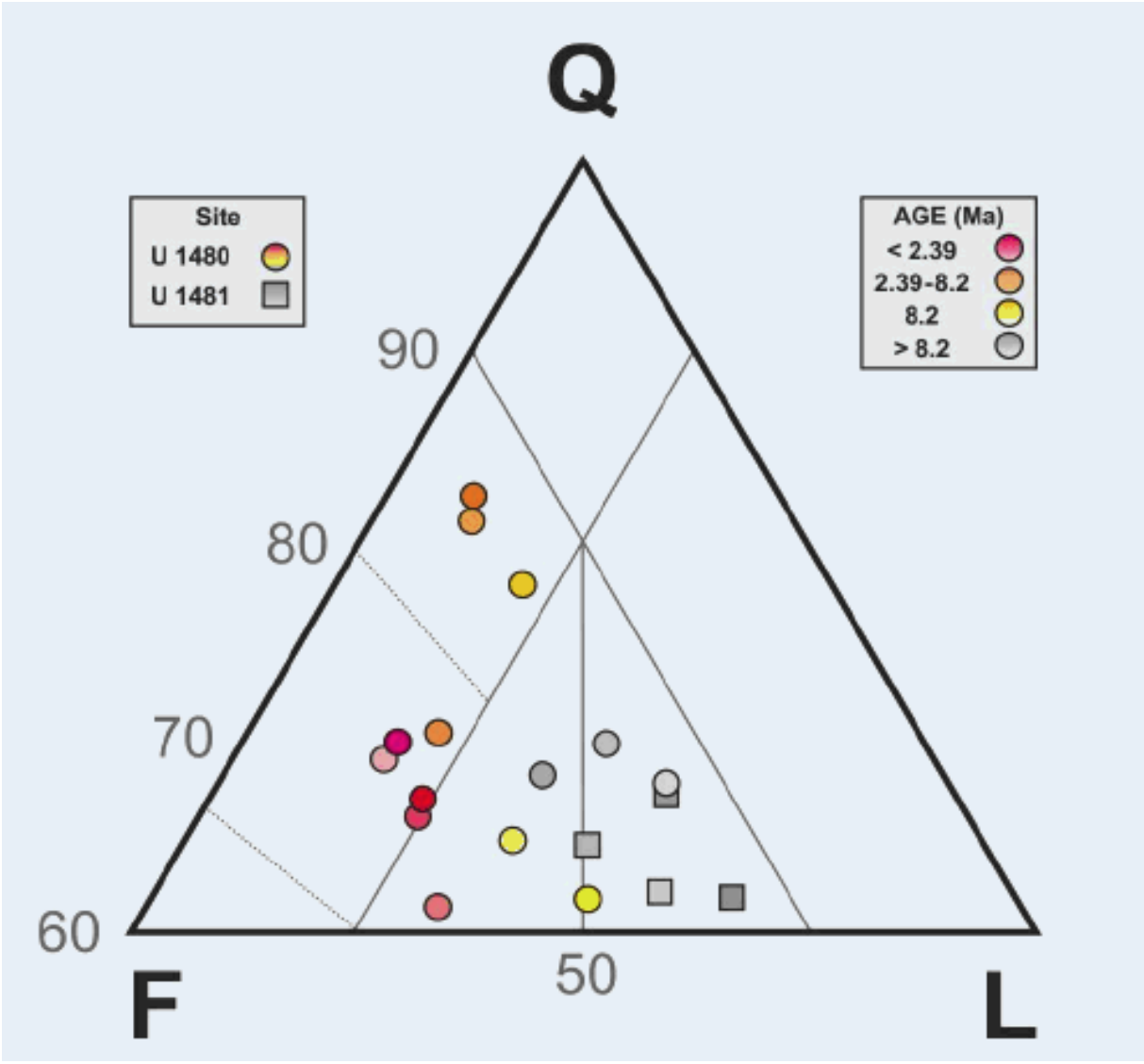

Figure 5

Click here to download Figure: Fig5_Pickering et al.pdf

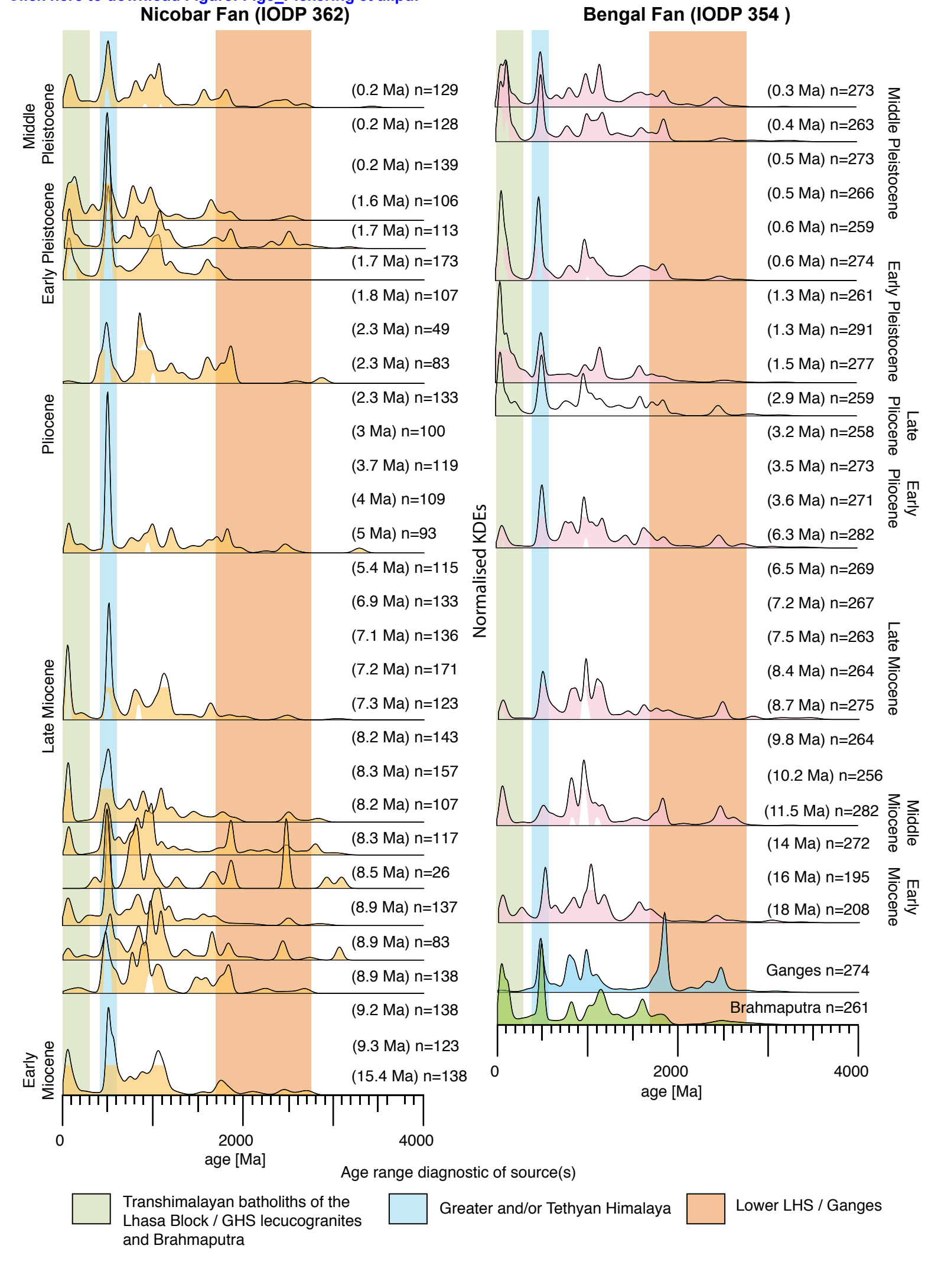

Figure 6

Click here to download Figure: Fig6_Pickering et al.pdf

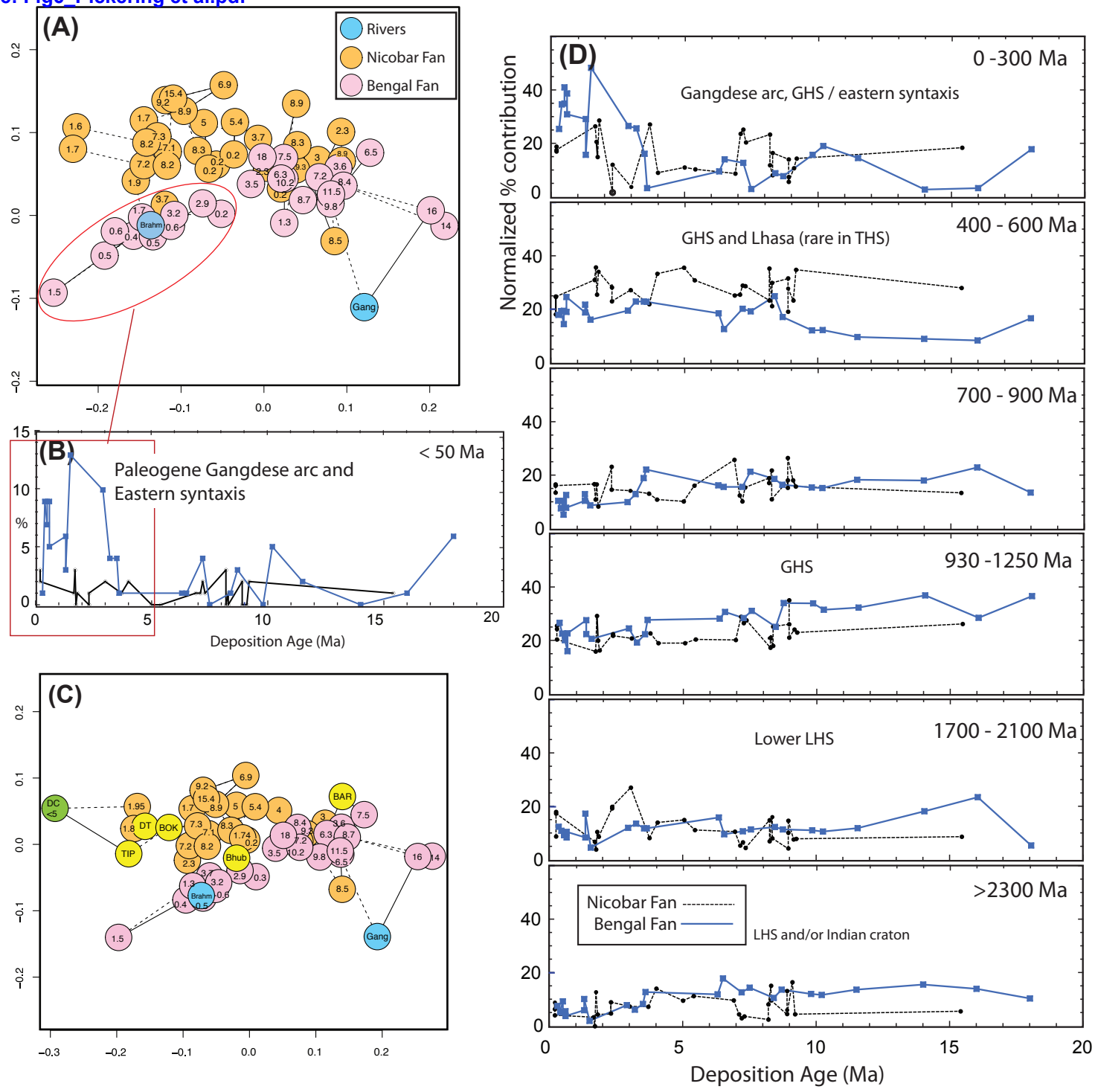

Figure 7
Click here to download Figure: Fig7_Pickering et al.pdf

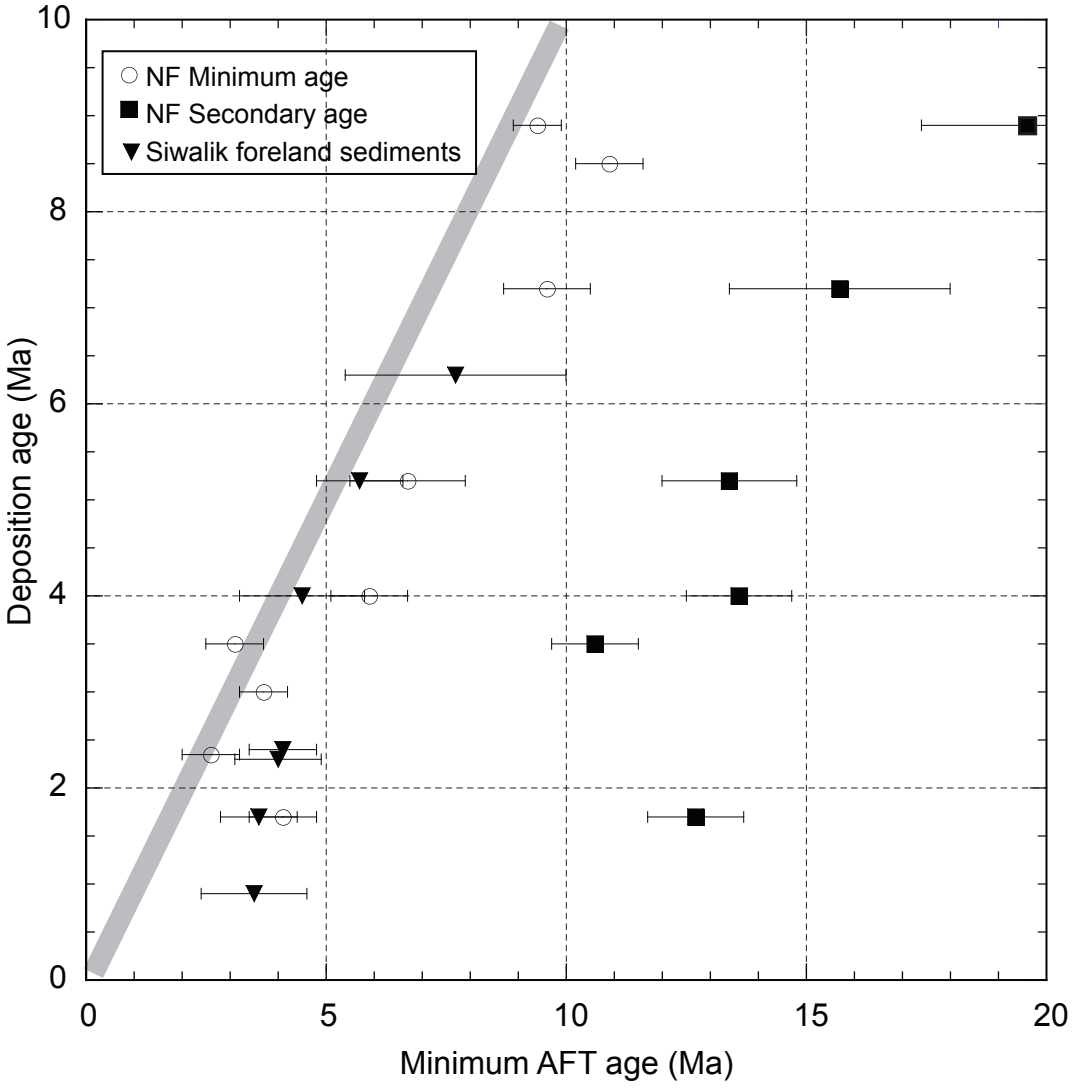

Figure 8

Click here to download Figure: Fig8_Pickering et al.pdf

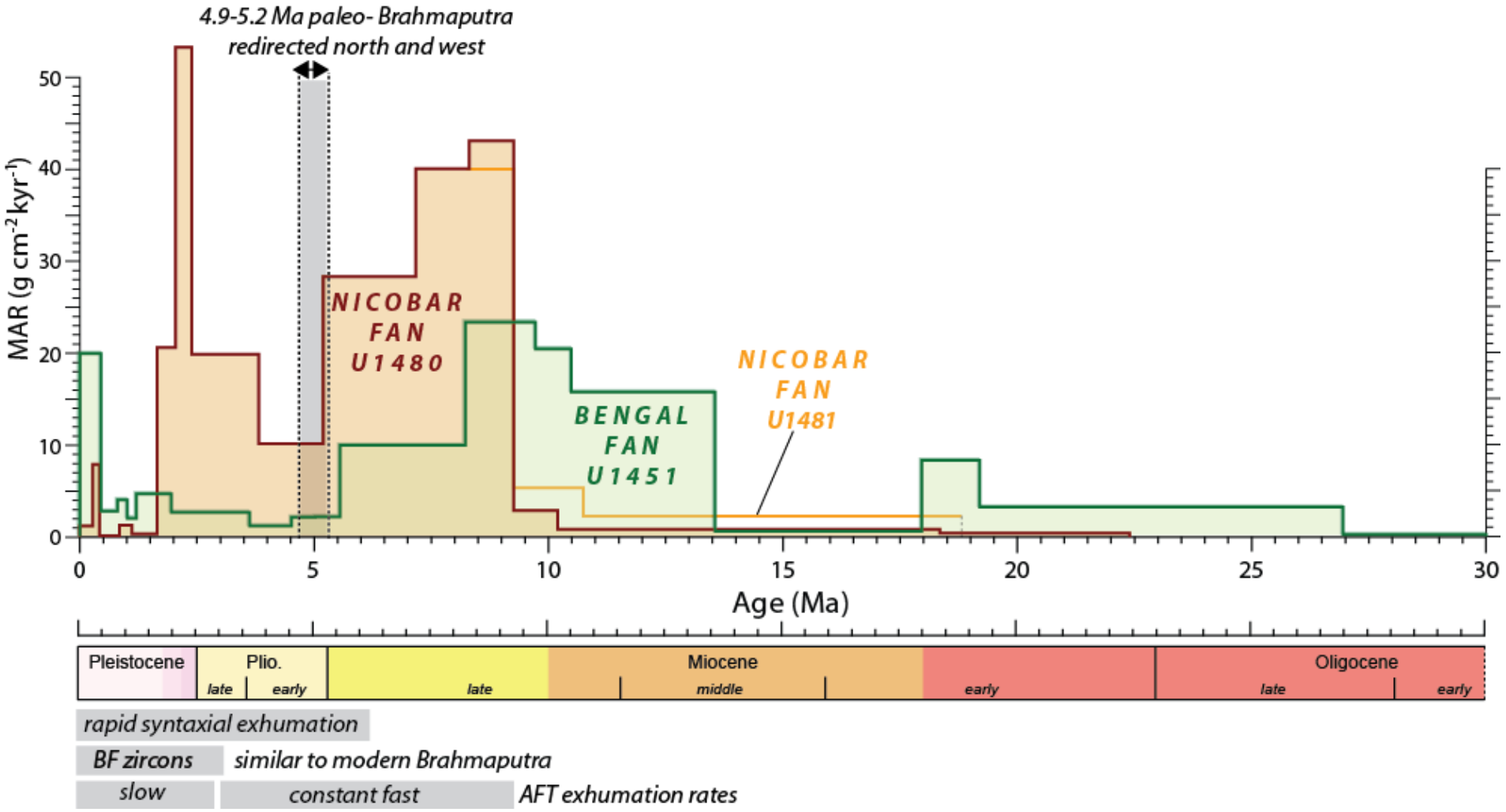

Figure 9

Click here to download Figure: Fig9_Pickering et al.pdf

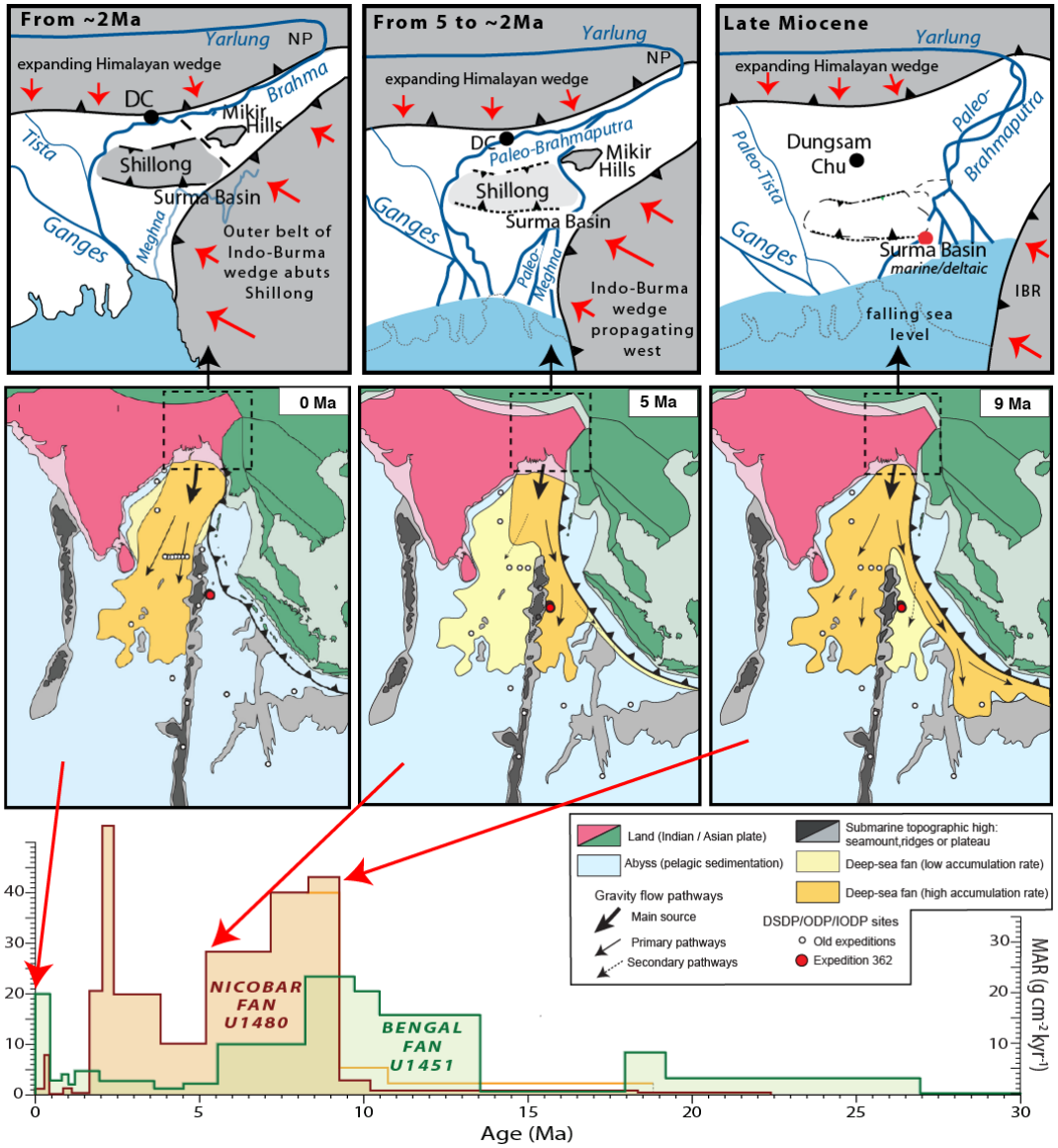

Table 1

Click here to download Table: Table 1_Pickering et al 2019.doc

Lab No	Deposit-ional Age	No. of grains	Central Age (Ma)	Age dispersion	Minimum Age (Ma)	Secondary Age (Ma)	Siwalik in Arunchal	Siwalik Eastern Bhutan
	0.9						3.5±1.1	
362-3	*1.6*	*66*	*7.1±0.9*	*56%*				
362-4	*1.7*	*30*	*4.8±0.8*	*84%*				
362-39	*1.7*	*50*	*5.2±0.7*	*68%*				
Combined	1.65	146	5.9±0.5	76%	4.1±0.7	12.7±1.1		3.6±0.8
362-8	*2.3*	*65*	*5.6±0.6*	*72%*			4.0±0.9	
362-11	*2.4*	*28*	*9.5±3.4*	*182%*				
Combined	2.35	93	7.0±1.1	138%	3.5±0.6			4.1±0.7
362-12	3.0	31	3.7±0.5	20%	3.7±0.5			
362-13	3.5	48	7.9±2.9	251%	3.1±0.6			
362-14	4.0	47	6.4±0.6	41%	5.9±0.8			4.5±1.3
362-15	*5.0*	*41*	*6.8±0.8*	*55%*				
362-16	*5.4*	*55*	*9.1±0.7*	*38%*				
Combined	5.2	96	8.2±0.6	47%	6.7±1.2	13.4±1.4		5.7±0.9
	6.3						7.7±2.3	
362-22	7.2	85	9.1±0.7	38%	9.6±0.9	15.7±2.3		
362-43	8.5	52	10.9±0.7	9%	10.9±0.7			
362-35	*8.9*	*45*	*8.9±0.6*	*8%*				
362-44	*8.9*	*21*	*9.0±1.1*	*7%*				
362-45	*8.9*	*50*	*9.5±0.9*	*44%*				
362-46	*9.0*	*61*	*11.8±1.0*	*36%*				
Combined	8.95	177	10.1±0.5	33%	9.4±0.6	19.6±2.6		

Supplementary material for online publication only

Click here to download Supplementary material for online publication only: Supplementary Section_Pickering et al 2019.doc

***Declaration of Interest Statement**

Declaration of interests

Yes The authors declare that they have no known competing financial interests or personal relationships that could have appeared to influence the work reported in this paper.

NONE The authors declare the following financial interests/personal relationships which may be considered as potential competing interests:

We, the autrhors, have no known competing financial interests or personal relationships that could have appeared to influence the work reported in this paper.

We have no financial interests/personal relationships which may be considered as potential competing interests.